Hydrogen in *N*-Methylacetamide: Positions and Dynamics of the Hydrogen Atoms Using Neutron Scattering

Heloisa N. Bordallo,*,†,‡ Dimitri N. Argyriou,† Mariette Barthès,§ Walter Kalceff,|| Stephane Rols,‡,§ Kenneth W. Herwig,⊥ Carlos Fehr,† Fanni Juranyi,▽,# and Tilo Seydel‡

Hahn-Meitner-Institut, Glienicker Strasse, 100 14109 Berlin, Germany, Institut Laue-Langevin, BP 156, 38042 Grenoble Cedex 9, France, Université Montpellier II, cc 26, 34095 Montpellier Cedex 05, France, Department of Physics and Advanced Materials, University of Technology Sydney, NSW 2007, Australia, Spallation Neutron Source, Oak Ridge National Laboratory, Tennessee 37831, Physical Chemistry, Saarland University, 66123 Saarbrucken, Germany, and Laboratory for Neutron Scattering, Paul Scherrer Institut, 5232 Villigen, Switzerland

Received: December 12, 2006; In Final Form: May 3, 2007

This work reports neutron diffraction and incoherent neutron scattering experiments on *N*-methylacetamide (NMA), which can be considered the model building block for the peptide linkage of polypeptides and proteins. Using the neutron data, we have been able to associate the onset of a striking negative thermal expansion (NTE) along the *a*-axis with a dynamical transition around 230 K, consistent with our calorimetric experiments. Observation of the NTE raises the question of possible proton transfer in NMA, which, from our data alone, still cannot be settled. We can only speculate that intermolecular repulsive forces increase as the O···H distance decreases upon cooling, and that around 230 K the lattice relaxes without observation of an actual proton transfer. However, the existence of a nonharmonic potential, reflected by the behavior of the phonon vibrations together with the observation of NTE, could be justified by the "vibrational" polaron theory in which a dynamic localization of the vibrational energy is created by coupling an internal molecular mode to a lattice phonon. More generally, this work shows that neutron powder diffraction techniques can be very powerful for investigating structural deformations in small peptide systems.

Introduction

Hydrogen bonds (HB) are partially covalent interactions between a hydrogen atom bound to an electronegative atom and an electronegative acceptor atom.[1] As they play an important role in defining the structure and function of biological macromolecular systems, understanding hydrogen-bonding energetics is a key factor for an accurate modeling of such interactions. However, a comparison with several molecular mechanics force fields widely used in molecular dynamics simulations of proteins, nucleic acids, and small molecules reveals systematic deviations from electronic structure calculations and protein structure statistics.[2,3] These results point toward the importance of understanding the anharmonic mode coupling of the amide group, present in the HB found in protein side chains and main chains. As these systems are so large and have a very intricate energy landscape, we need to model smaller prototypical systems in order to understand these interactions. One of the longstanding building block models of the repeated peptide linkage of polypeptides and proteins is *N*-methylacetamide ($CH_3CONHCH_3$, hereafter referred to as NMA), a single amide containing methyl groups at both extremities. Structure and vibrational studies of NMA have been the subject of a number of experimental and theoretical investigations.[4−7] Of particular interest in these studies are the possible relationships between vibrational signatures of amide modes of this model peptide and those of secondary structures of peptides and proteins.

NMA, which is highly hygroscopic, melts just above room temperature (301 K). The structure of crystalline NMA has an almost planar symmetry, with the NH group of one molecule bonded to the CO group of the neighboring one. Single-crystal neutron diffraction data below and above the known structural phase transition around[8] $T' = 274$ K indicates that the high-temperature phase crystallizes in the noncentrosymmetric space group $Pn2_1m$. On the other hand, and in agreement with X-ray structural determination,[9] the lower temperature phase shows methyl groups slightly rotated out of the $y = 0$ plane and a $Pn2_1a$ structure. A schematic view of the structure is shown in Figure 1. ^{13}C NMR studies[10] exhibit the coexistence of typical broad lines with very narrow bands, indicating that dynamic disorder is present at temperatures well below that of the structural transition. This suggests an averaging of quadrupolar interactions of the N-atom by rapid motion of a disordered state in the solid phase. The dynamic disorder evident in the ^{13}C NMR data is also reflected in unusually large thermal parameters of the carbon atoms derived from diffraction data collected at 250 K.[4] Furthermore, recent structural information has suggested the possibility of a glassy-type disorder[11] below T', as well as the occurrence of a second phase transition[4] in the vicinity of 230−240 K.

Small but significant differences are found in protein structures measured at cryogenic temperatures when compared with ones obtained at room temperature.[12] With this application to

* Corresponding author. Telephone: +49 (0)30 8062 2924. Fax: +49 (0)30 8062 2781. E-mail: bordallo@hmi.de.
† Hahn-Meitner-Institut.
‡ Institut Laue-Langevin.
§ Université Montpellier II.
|| University of Technology Sydney.
⊥ Oak Ridge National Laboratory.
▽ Saarland University.
Paul Scherrer Institut.

10.1021/jp068528z CCC: $37.00
Published on Web 06/16/2007

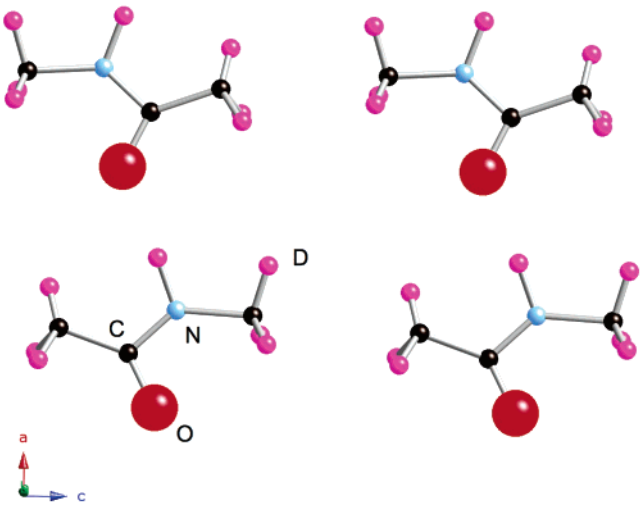

Figure 1. Schematic view of crystalline *N*-methylacetamide ($CH_3-NH-CO-CH_3$, or NMA) showing the one-dimensional chains with H-bonds between amide groups of neighboring molecules. The N—H···O=C chains may be viewed as a model system for proteins.

real biological systems, it is very important to reinvestigate the crystal structure of the model NMA as a function of temperature, paying special attention to the effect of cooling rate on the solid-state transition. A full understanding of the origin of these structural transitions depends on probing the relationship between local dynamics of the methyl groups[13] and the molecular structure of NMA. In this paper we present an extensive neutron scattering study of the methyl motion in a wide dynamical range of time, as well as neutron diffraction measurements on fully deuterated NMA. We find that in NMA the dynamical rotational motion of the methyl groups is activated around 100 K. Moreover, using the Fine Resolution Powder Diffractometer E9 at the Hahn-Meitner-Institut (HMI) and the High Resolution Powder Diffractomer (HRPD) at ISIS, we show that a second structural transition occurs around 230 K, which is characterized by the onset of a clear negative thermal expansion (NTE) of the *a* lattice parameter. We interpret that the NTE is a result of anharmonicity of the interatomic potential that is reflected in the unusual lattice dynamical features of the amide groups in NMA.[14]

Experimental Section

A. Materials and Methods. Considering that the intensity of the vibrational spectra obtained by means of neutron scattering is simply given by the product of the amplitude of the motion with the known scattering cross section of a nucleus, summed over all atoms of the system, it is of particular significance in the present work that the scattering cross sections of hydrogen (H) and deuterium (D) differ by a factor of 20. In this context isotopic replacements cause significant changes of the observed intensities, and can thus be employed to differentiate the motion of a specific H-atom (or group of atoms). Therefore, to shed light on the dynamics of the different H-groups in NMA, quasi-elastic neutron scattering (QNS) data were obtained on $CH_3CONHCD_3$, $CD_3NHCOCH_3$, $CH_3NDCOCH_3$, and $CD_3NDCOCD_3$. To minimize the effects of multiple scattering during the QNS measurements, a sample of thickness corresponding to a transmission value of about 0.9 was used.

Neutron powder diffraction (NPD), with its ability to directly reveal the position of light atoms by virtue of their different scattering lengths, offers a great potential for investigating the geometry of hydrogen-bonding systems. Unfortunately, its use on protonated samples frequently faces a specific technical difficulty: the large incoherent scattering of H results in background scattering that greatly reduces the signal-to-noise ratio of the data, making it difficult to detect coherent Bragg scattering from the sample. In our work these difficulties were overcome by the use of a fully deuterated sample. We present here diffraction data obtained on 2 g of $CD_3NDCOCD_3$ synthesized by CDN Isotopes (Vandreuil, Quebec) with purity greater than 99%. The samples were loaded into their containers in a glovebag flooded with helium. To avoid the inclusion of disorder in the structure, instead of pulverizing the sample as described in ref 5, we chose for the E9 experiments to quench it down to 20 K and perform the measurement in steps of 20 K on heating until just below the melting point, i.e., 280 K. However, due to the fast recrystallization of NMA and consequent formation of various crystallites with different preferential orientations, the data collection was carried out by rotating the sample about its axis (using three different orientations), and the analysis was performed on the averaged data. A different approach was followed for the HRPD experiments measured only at 140 K: the sample was loaded into a sample holder containing small pieces of fiberglass, providing for a large number of nucleation centers and ensuring that the recrystallization of NMA occurred with a large number of randomly oriented grains, giving the powder data a high degree of averaging.

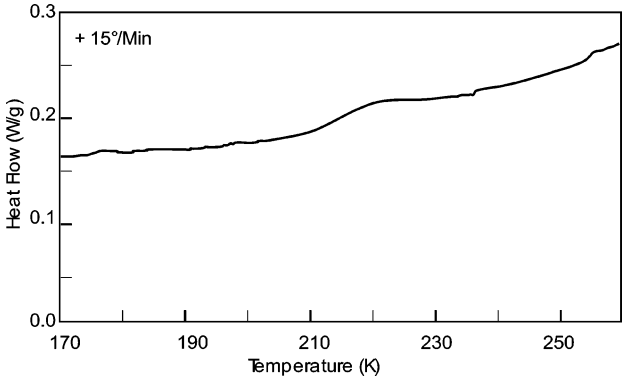

Figure 2. DSC heating scan showing a very weak anomaly around 220 K (~ −50 °C), indicating that a second structural transition may occur in NMA.

B. Calorimetric Results. Differential scanning calorimetry (DSC) measurements obtained on heating at +15°/min are given in Figure 2. We can observe that, in agreement with earlier work,[4] besides the first-order transition that takes place at $T' =$ 274 K, a very weak anomaly around 220 K (~ −50 °C) indicates that a second structural transition may occur.

C. Neutron Scattering Measurements. NPD experiments were carried out over a wide temperature range, from 20 to 300 K on a fully deuterated sample, $CD_3CONDCD_3$, using the dedicated fine-resolution powder diffractometer E9 at the Hahn-Meitner Institut (Berlin, Germany). This instrument provides good efficiency by virtue of its 64 ^{3}He detectors distributed over a 160° range in scattering angle, while good resolution ($\Delta d/d \sim 2 \times 10^{-3}$) derives from a multicollimator of 10 ft horizontal acceptance. Data are collected by step-scanning the 2.5° interval from one collimator to the next. Further experiments at 140 K were performed using HRPD, the High Resolution Powder Diffractometer at ISIS (Didcot, U.K.). The HRPD resolution in the main backscattering detector bank, with $\Delta d/d \sim 4 \times 10^{-4}$ (which is effectively constant over the wide *d*-spacing range available) gives a unique capacity for the study of structural

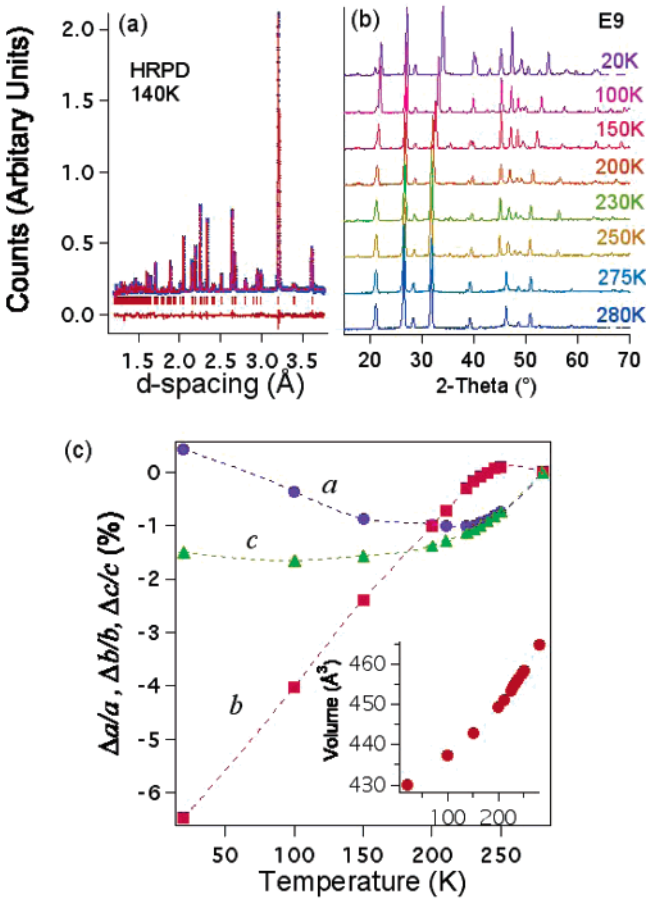

Figure 3. (a) Rietveld analysis of neutron powder diffraction data for fully deuterated NMA ($CD_3CONDCD_3$), measured on the HRPD diffractometer at ISIS. The data are shown as crosses while the continuous line through the data is the calculation of the diffraction pattern using the $Pn2_1a$ model. The difference between the observed and calculated patterns is shown as the bottom trace; the vertical lines below the data indicate the expected positions of Bragg reflections for the $Pn2_1a$ structure. (b) Neutron diffraction patterns of fully deuterated NMA ($CD_3CONDCD_3$) for a range of temperatures measured on the E9 diffractometer at BENSC. (c) Lattice constants of NMA determined by combining Rietveld refinements and Le Bail fitting and assuming the orthorhombic cell.[30] The lattice constants are shown as percent changes with respect to measurements at 280 K (e.g., $\Delta a/a = (a(T) - a(280\ \mathrm{K}))/a(280\ \mathrm{K})$ %). The lattice constants at 280 K are $a = 9.721(1)$, $b = 6.5268(4)$, and $c = 7.298(1)$ Å). The inset shows the unit cell volume as a function of temperature.

details such as subtle phase transitions. The powder diffraction data were analyzed using the Rietveld method and the program GSAS.[15] In the analysis it was found that the E9 data suffered from preferred orientation from several large crystallites. Although this did not hamper the accurate determination of lattice constants, it did prohibit the analysis of Bragg intensities. To obtain the temperature dependence of the lattice constants from these data, we employed a method of first refining the powder data on the basis of the known crystallographic structure to get correct peak positions, and then using Le Bail's technique to improve the fit and thus the accuracy of the lattice constants. The HRPD data, shown in Figure 3a, showed no evidence of preferred orientation, and the full structure of NMA could be refined along with the cell constants at 140 K.

QNS experiments were performed using the time-of-flight (ToF) spectrometer FOCUS at the Paul Scherrer Institute (PSI, Villigen, Switzerland) using a wavelength $\lambda = 5.75$ Å, corresponding to elastic energy resolutions ΔE of 50 μeV (full width at half-maximum (fwhm)).[16] The highly hygroscopic samples ($CH_3CONHCD_3$ and $CD_3NDCOCD_3$) were placed under helium on a flat, rectangular aluminum slab of 0.2 mm thickness. The detector banks in this instrument cover the angular range $10° < 2\theta < 130°$, giving access to momentum transfers of $0.2\ \text{Å}^{-1} < Q < 2\ \text{Å}^{-1}$ at $\lambda = 5.75$ Å. The samples were placed in the standard Orange cryostat, and the temperature was varied between 2 and 300 K. Also, in order to analyze the short-time dynamics (inelastic response) of the CH_3 groups, we obtained the generalized density of states.[17]

As previously reported,[13] QNS data on $CH_3CONHCD_3$ and $CD_3CONHCH_3$ were also obtained using the QENS spectrometer at the Intense Pulsed Neutron Source (IPNS)[18] with an energy resolution of 85 μeV. The sample was confined to an annular volume between two aluminum cylinders in a glovebag flooded with helium. Furthermore, $CH_3CONDCH_3$ was measured on the cold neutron backscattering spectrometer IN10 located at the Institut Laue-Langevin (ILL, Grenoble, France), using an unpolished Si(111) monochromator and analyzer crystals corresponding to a wavelength of 6.27 Å, thereby achieving an energy resolution ΔE of about 1 μeV (fwhm), corresponding to times of a few nanoseconds. Seven ^{3}He detector tubes were installed evenly spaced in 2θ, giving access to momentum transfers of $0.4\ \text{Å}^{-1} < Q < 1.95\ \text{Å}^{-1}$. The energy transfer scans for QNS measurements on IN10 were recorded by moving the monochromator along its surface-normal direction on a sinusoidal velocity profile with a frequency of 10 Hz and thus Doppler-shifting the monochromatic neutrons. The detected neutrons were accordingly sorted into 256 discrete channels corresponding to their energy transfer.

Spectra correction, normalization, grouping, and transformation to the energy transfer scale were performed using standard routines available at PSI, IPNS, and ILL. All spectra were corrected by normalization of the detectors with vanadium and subtraction of the empty cell scattering. For the FOCUS and IN10 experiments the angle between the plane of the sample and the incident neutron beam was 135°.

In addition, incoherent elastic neutron scattering measurements were performed on IN10 using the fixed-window technique in the temperature range 20−305 K. During these measurements, the neutron-scattered intensity is monitored within a narrow energy range (whose width is given by the instrumental resolution) centered at $\omega = 0$, as a function of temperature and scattering vector Q; only those neutrons that are elastically scattered are counted. Data were collected during cooling and during heating over 16−24 h. No statistically significant differences were observed between the two sets of data.

D. Neutron Scattering Theory. Incoherent neutron scattering experiments provide information on the energy transfer and neutron scattering distribution for a solid angle. Depending on the temperature and energy resolution (time) range, the measured scattering function $S(Q,\omega)$, where Q is the magnitude of the scattering wave vector and ω is the energy transfer, will express different contributions. This function can be decomposed into three components: elastic, quasi-elastic (QE), and inelastic, as follows:[19]

$$S(Q,\omega) = S_{\mathrm{elastic}}(Q,\omega{=}0) + S_{\mathrm{quasi}}(Q,\omega) + S_{\mathrm{inelastic}}(Q,\omega) \quad (1)$$

The elastic component originates from neutrons without change in energy, and the inelastic component is related to vibrational modes.[14] QE scattering, which is a broadening of the elastic peak, describes the dynamical nature of the molecular motion, and in this particular study is dominated by the incoherent cross section of the hydrogen. Thus, to address the

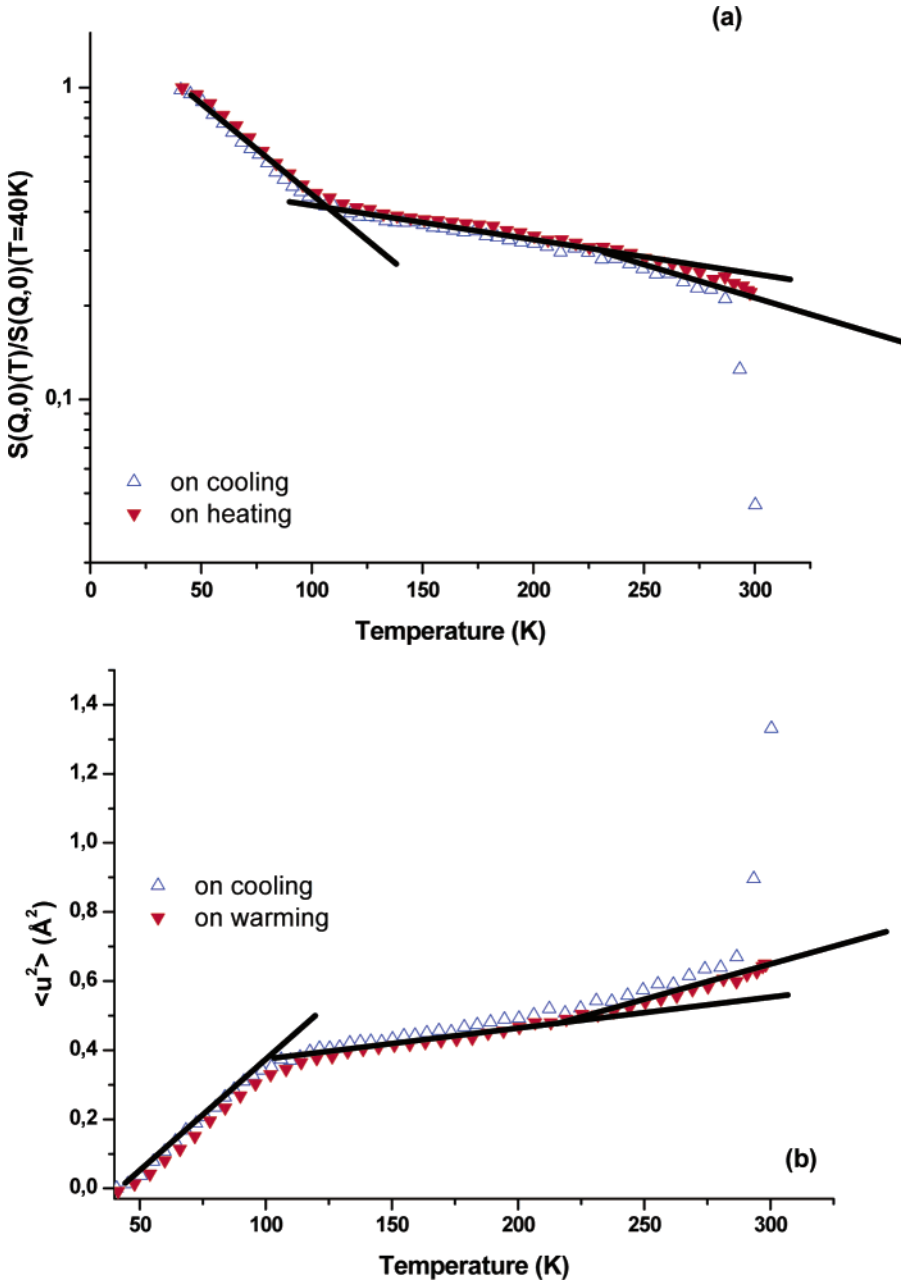

Figure 4. (a) Elastic scattered incoherent intensity of $CH_3CONDCH_3$ at $Q = 0.5$ Å^{-1} normalized to 40 K. (b) Average mean square hydrogen displacement versus temperature obtained from the analysis of $S(Q,0)(T)/S(Q,0)(T=40\text{ K})$. The sample was cooled to 40 K (blue △) then heated above the melting point (red ▼). IN10 has an energy resolution corresponding to motions faster than 4 ns.

different motions of the CH_3 groups in NMA, the QE response was probed in two different time scales. Fast motions, in the range of hundreds of picoseconds, were probed using QENS and FOCUS, while motions on the order of a few nanoseconds were studied using IN10 at ILL.

To get an insight into the possible dynamical transition behavior due to the temperature dependence of the anharmonic motions in NMA, we probed the elastic incoherent scattering intensity $S_{inc}(Q,\omega=0)$. As the occurrence of a molecular motion on the time scale of the backscattering spectrometers like IN10 at a given temperature induces QE broadening of the scattering function, and consequently a reduction of the detected elastic intensity, the so-called "fixed energy window" measurements detect only scattered neutrons that do not exchange energy with the sample within the energy resolution of the instrument.[20] At low temperatures the linear decrease of the normalized elastic scattering, $[S(Q,0)(T)/S(Q,0)(T\sim0)]$, on a logarithmic scale, is described by the Debye−Waller factor.[21]

$$S(Q,\omega\approx0) = \exp^{(-\langle u(T)^2\rangle Q^2/3)} \qquad (2)$$

where $\langle u(T)^2\rangle$ is the mean square displacement of the atoms around their equilibrium positions. Due to the larger incoherent cross section of the hydrogen, the measured $\langle u^2\rangle$ corresponds in practice to the H-atoms. Using the "frequency window" model, it is expected that if a dynamical transition takes place the temperature dependence of dynamical relaxation processes will cause a change in slope of the observed $\langle u^2\rangle$. This behavior is entirely due to the temperature dependence of the motional time scales.

Results and Discussion

A. Structural analysis of NMA-d_7 ($CD_3CONDCD_3$). Figure 3b shows a set of diffraction scans referenced to λ =

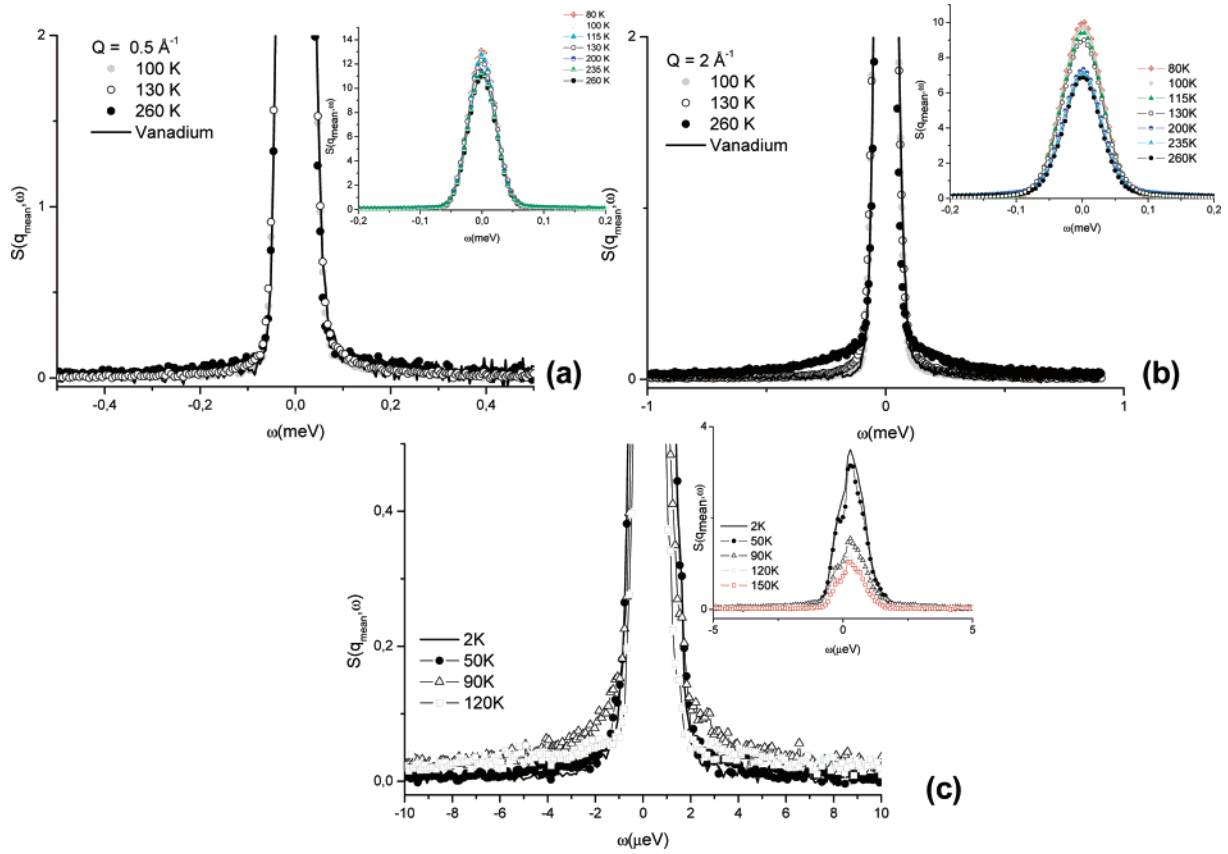

Figure 5. Dynamic structure factors obtained over a range of temperatures for each sample. The data were averaged over the whole *Q*-range. (a, b) Rescaled C−CH_3 spectra obtained using FOCUS for $\Delta E = 50$ μeV, shown at 260 (●), 130 (○), and 100 K (gray ●), for the elastic *Q* values (a) 0.5 and (b) 2 Å^{-1}. (c) Rescaled C−CH_3 spectra obtained using IN10 for $\Delta E = 1$ μeV at 120 (□), 90 (△), and 50 K (●), for the elastic *Q* value 1.2 Å^{-1}; the solid line is the measured resolution function. The inset shows the corresponding elastic intensity at various temperatures. As expected, the elastic intensity decreases as the intensity of the QE component increases.

1.797 30 Å using E9 at temperatures ranging from 280 to 20 K and normalized on the strongest peak, occurring near $2\theta = 26°$. Pronounced changes in the diffraction pattern between 275 and 250 K are observed, consistent with the structural phase transition at $T' = 274$ K reported by various authors[4,5,8,9] from space group $Pn2_1a$ below the transition to $Pn2_1m$ above it. As shown in Figure 3a, the data measured on HRPD at 140 K were consistent with the $Pn2_1a$ structure.

The temperature dependence of the lattice constants shows a particularly interesting behavior as shown in Figure 3c. First, there is a significant step in the *b*-parameter around T', below which all three lattice constants decrease with temperature. However, for the *a*- and *c*-axes a markedly different behavior develops between 230 and 150 K in which the *a*-axis shows an NTE while the *c*-axis shows in comparison a weaker temperature dependence. This behavior is consistent with the calorimetric results, indicating the presence of yet another phase transition. Over the measured temperature range, the volume shows a contraction of the unit cell of 8%. Several inorganic materials displaying NTE are known, with the most spectacular examples of volume NTE found in the ZrW_2O_8 family,[22] but the number of organic examples is very limited.[23,24] In general, NTE is unusual in solids and it is indicative of significant anharmonic effects or frustration.[25] From the powder diffraction data alone we cannot completely explain the mechanism of NTE along the *a*- and *c*-axes. However, we can speculate that anisotropy of the lattice strain can be correlated to molecular packing and the direction of the intermolecular HB in the structure. The "softest direction" (along the crystallographic *b*-axis) is normal to the molecular layers, while the lowest compressibility is observed along the backbone (crystallographic *c*-axis). Similar behavior has been observed in polymorphs of glycine[26] and paracetamol.[27] Furthermore, one expects that NTE will reflect the anharmonicity of the potential near its minimum, and that at higher temperatures activated motions become more frequent. This fast librational process should then give rise to an excess expansion and is seen as a nonlinear contribution to the temperature dependence of the atomic mean square displacements. These fast local motions are expected to give rise to QNS spectra in NMA.

B. Using Selective Deuteration To Probe the Motion of the Nonequivalent Methyl Groups in NMA. As discussed earlier, the QENS data ($\Delta E = 85$ μeV) exhibit a thermally activated QE broadening in $CH_3CONHCD_3$ (C−CH_3) and CD_3-$CONHCH_3$ (N−CH_3) at temperatures above 100 K.[13] Assuming that the QE scattering arises mainly from the reorientational motion of the methyl groups, we were able to deduce the energy of activation (*E*) for each methyl group using an Arrhenius-like model, obtaining E(C−CH_3) = 7.41 kJ/mol and E(N−CH_3) = 4.52 kJ/mol. The fact that these activation energies are different indicates that the dynamical environments of the two unique methyl groups are different. From these results we could conclude that the disorder previously observed by ^{13}C NMR in NMA is connected to dynamical rotational disorder in the chains around the C−C axis. Furthermore, the reorientation of the CH_3 groups is highly dependent on the local arrangement.

C. Different Dynamical Regimes As Evidenced by Elastic Measurements. Results obtained from the fixed-window scans on partially deuterated NMA ($CH_3CONDCH_3$) are presented in Figure 4a. Evaluating the *Q* dependence of [$S(Q,0)$](T)/$S(Q,0)$

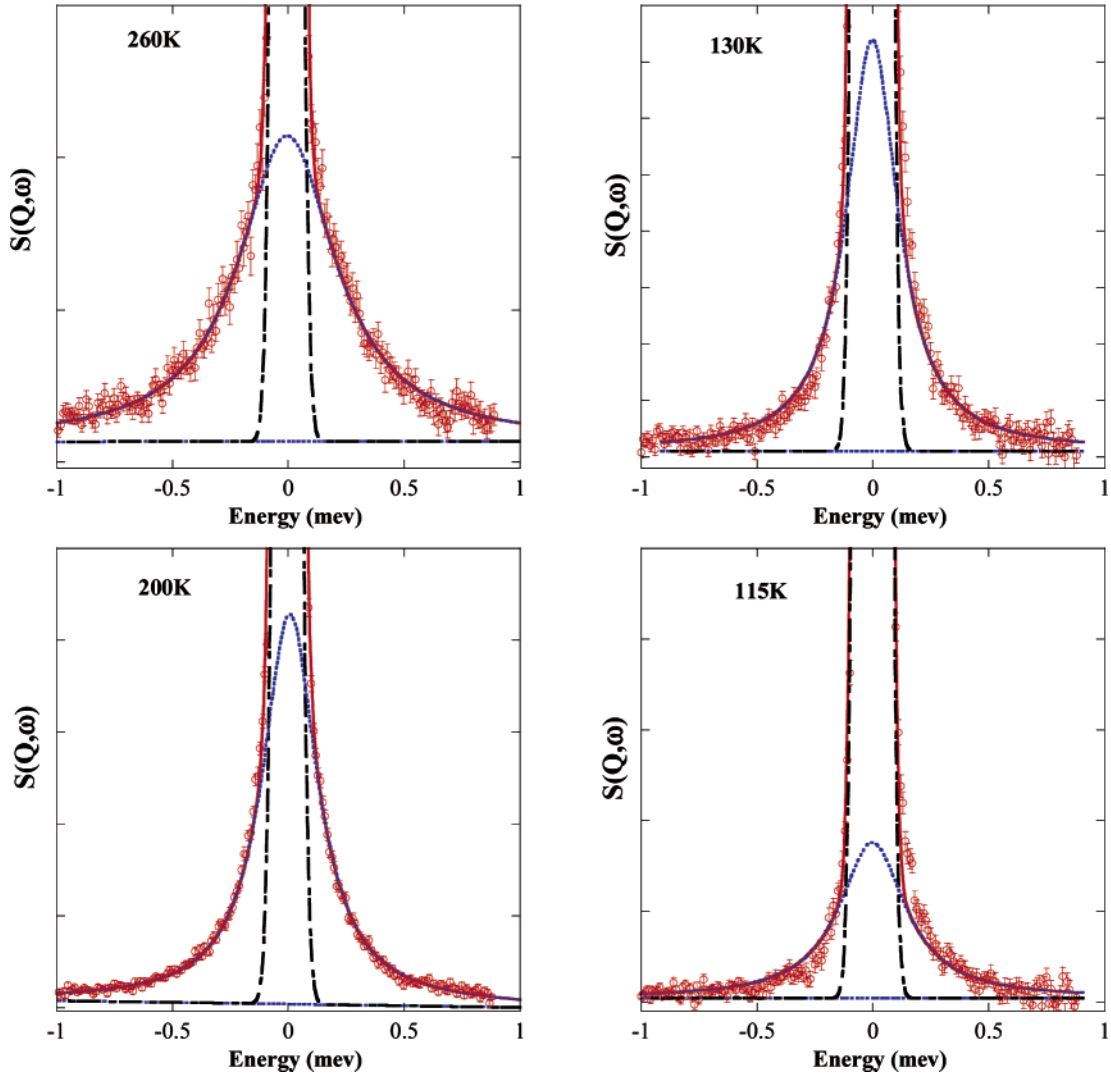

Figure 6. Examples of FOCUS experimental spectra (○) for C−CH_3 at selected temperatures for $Q = 1.65$ Å^{-1}, $\Delta E = 50$ μeV, together with the best fit (solid lines) and the QE component (dotted lines). The background and the resolution function are also shown (dotted lines and long dashed lines, respectively).

at $T = 40$ K, we calculate the $\langle u^2 \rangle$ shown in Figure 4a,b. In Figure 4a,b, two inflection points are clearly observed: one near 100 K and the second in the vicinity of 230−240 K. By taking into account the large temperature interval separating the changes in the slope of $\langle u^2 \rangle$, it appears that differences in the characteristic times of the two motions are genuine.[28] Indeed, as seen in Figure 5a,b, the QE spectra of $CH_3CONHCD_3$ obtained using $\Delta E = 50$ μeV, show the following:

(i) As expected, the effect of CH_3 rotation dynamics is clearly observed in the higher-Q spectra in this time range. Also, heating the sample leads to a concomitant increase in both the QE intensity and broadening, thus confirming that the CH_3 motions are activated around 80 K.

(ii) On the other hand, the existence of a slow dynamic process appears as an elastic component superimposed on the quasi-elastic broadening related to CH_3 orientational motions (see inset of Figure 5). This contribution is represented by the purely elastic term ($\delta(\omega)$ in eq 3, below) and can be related to motions occurring on a longer time scale compared to the instrumental resolution. It is worth noting that the slow dynamics is better observed at high Q-values and lower temperatures.

In order to check whether the apparent elastic peak observed in the FOCUS experiment contains a narrow QE component related to slow CH_3 motions, we carried out high-resolution measurements with the backscattering spectrometer IN10 at the ILL. As shown in Figure 5c, the IN10 spectra obtained for $CH_3CONDCH_3$ indeed reveal the existence of a slow dynamic process. It can be seen that QE broadening is clearly evident only between 120 and 90 K, indicating that the slower motion "moves out" of the experimental frequency window. This qualitative effect is perhaps an indication that the lowest transition is basically activated and involves an energy-barrier crossing.[29]

(i) Analysis of the Methyl Rotational Motion in NMA. To obtain a qualitative description of the hydrogen motions in $CH_3CONHCD_3$, the FOCUS + IN10 spectra were fitted assuming an approximated Dirac function and a single Lorentzian line width to describe the elastic and QE signals, as follows:

$$S_m(Q,\omega) = [A_0(Q)\,\delta(\omega) + (1 - A_0(Q))L_i(\Delta_i,\omega)] \otimes R(\omega) + B \quad (3)$$

where F is a scaling factor, A_0 represents the elastic incoherent structure factor, $L_i(\Delta_i,\omega)$ are Lorentzian functions describing the QE component, with a half-width at half-maximum (hwhm) Δ_i, and $R(\omega)$ is the experimental resolution function. $R(\omega)$ is described by either the vanadium run (FOCUS) or by the spectra at 2 K (IN10). B is a flat background term.

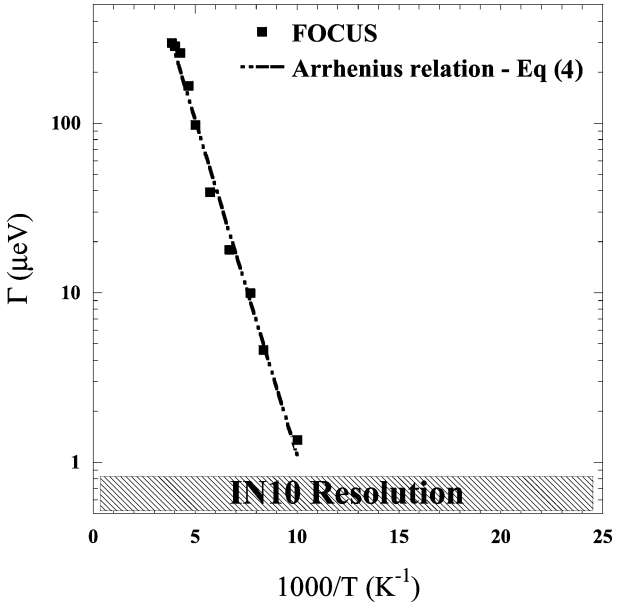

Figure 7. Lorentzian hwhm (Γ) obtained from the fits of CH_3-$NHCOCD_3$ using FOCUS ($\Delta E = 50$ μeV) QNS data. The variation with temperature of Γ was obtained using the model described in the text. The line corresponds to a low-temperature Arrhenius-like activation, $\Gamma = A_0 \exp(-\Delta E/kT)$. The shaded region represents the range of IN10 resolution, indicating that below 50 K existing motions in the range of a few nanoseconds can no longer be detected.

Figure 6 shows a typical QNS spectrum, obtained using FOCUS for $CH_3CONHCD_3$ for $Q = 1.65$ Å^{-1} with $\Delta E = 50$ μeV, together with the fitted curve obtained using the model described above. There is excellent agreement between the fitted model and the experimental data.

For reorientation motion, the QE broadening (Γ) is related to the activation energy by an Arrhenius relation,[19] as

$$\Gamma = \Gamma_0 e^{-E_{act}/kT} \qquad (4)$$

with Γ_0 and E_{act} being the attempt frequency and the activation energy, respectively. In this model it is inferred that the molecule oscillates about the equilibrium orientations for an average time τ and then moves to a new equilibrium orientation. The Arrhenius plot of the variation of Γ_0, obtained by combining the QNS data as a function of temperature, is shown in Figure 7. From this curve and expression 4, it is found that, for C−CH_3, Γ_0 is about 10 meV and $E_{act} = 7.5$ kJ/mol, in agreement with our previous result.[13] This latter value corresponds to typical values encountered in the literature for other molecular systems containing methyl groups.[30] These results indicate that in NMA the dynamical rotational disorder in the chains around the C−C axis persists until around 100 K.

Additionally, the prefactor $\Gamma_0 = 10$ meV suggests the possibility of the presence of a methyl group librational mode located in this frequency range, which should be observable as a peak in the vibrational density of states:[17]

$$G(Q,\omega) = \frac{M}{k_B T}\left(\frac{\hbar\omega}{Q}\right)^2 \exp\left(-\frac{\hbar\omega}{k_B T}\right) S(Q,\omega) \qquad (5)$$

M is the mass of the scattering units, k_B is Boltzmann's constant, T is the temperature, $\hbar\omega$ gives the neutron energy transfer, and $S(Q,\omega)$ is the experimental incoherent scattering function (here dominated by the H-motion). It is well-known that librational peaks are strongly damped with increasing temperature, and as a result the effective density of states, $g(\omega)$, for $CH_3CONHCD_3$ can be calculated from FOCUS data between 80 and 260 K. The results are reported in Figure 8, showing that indeed there is a very strong feature at 10 meV in the low-temperature spectrum. One can consider that this line might arise from a segmental libration of the whole CH_3 group around the backbone, and might be identified with the first librational mode of the methyl group.[31]

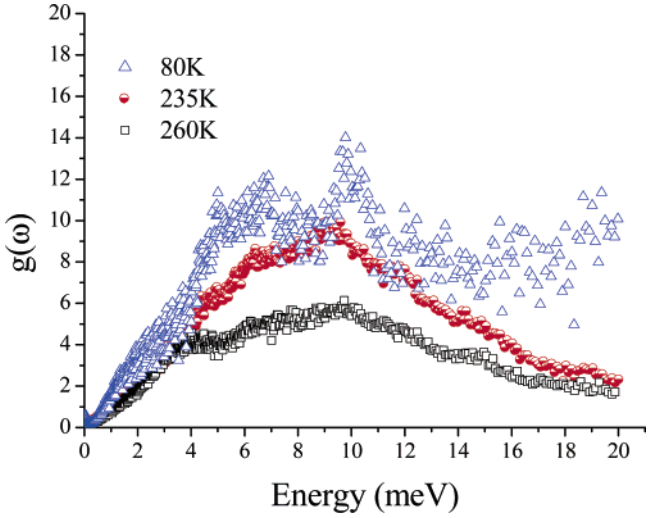

Figure 8. Inelastic neutron scattering spectra at various temperatures for $CH_3CONHCD_3$. The very strong feature at 10 meV observed in the low-temperature spectra can be assigned to segmental libration of the whole CH_3 group around the backbone.

Furthermore, it is interesting to note that for a perfect harmonic solid the generalized density of states should reveal the same spectrum for all temperatures; however, changes caused by disorder in the low-energy range below 10 meV cause a mixture of collective modes with local librational modes. These large-amplitude motions at low frequencies may be interpreted as resulting from a continuous shift of the density of states toward low frequencies as a consequence of a general softening of the structure,[32] and also may explain the behavior of the mean square displacement, $\langle u^2 \rangle$. The deviation of $\langle u^2 \rangle$ might then be attributed to a lack of long-range correlation, and in turn this extra inelastic scattering is assigned to boson behavior.[33]

(ii) Analysis of Picosecond to Nanosecond Dynamics. In order to analyze the IN10 data, the sum of two Lorentzian line shapes and a Dirac peak approximated by a narrow Lorentzian with fixed width has been used to fit the experimental spectra between 90 and 150 K. This sum has been convoluted numerically (approximated by a multiplication with the spectrometer matrix) with an analytical description of the resolution function as determined by the scattering from vanadium. Subsequently, a constant background has been added. From the Lorentzian line shapes, the corresponding relaxation times τ_i have been determined as shown in Figure 9. The backscattering spectra measured on IN10 probed two different motions, viz. a slow motion that presents a slight Q-dependence, with characteristic time of a few nanoseconds (corresponding to $\Delta_0 =$ tenths of microelectronvolts), and a faster one of ∼100 ps (corresponding to $\Delta_1 \sim 5$ μeV). The faster motion, which is Q-independent and barely resolved in the IN10 spectra above 120 K but comparable to the one probed using QENS and FOCUS, can be attributed to the rotational dynamics of the CH_3 groups. On the other hand, the interpretation of the slower component is complicated in view of the width of the QE broadening ($\Delta_0 <$ 0.6 μeV) with respect to the energy resolution ($\Delta E = 1.1$ μeV), making it difficult to unambiguously attribute this QNS

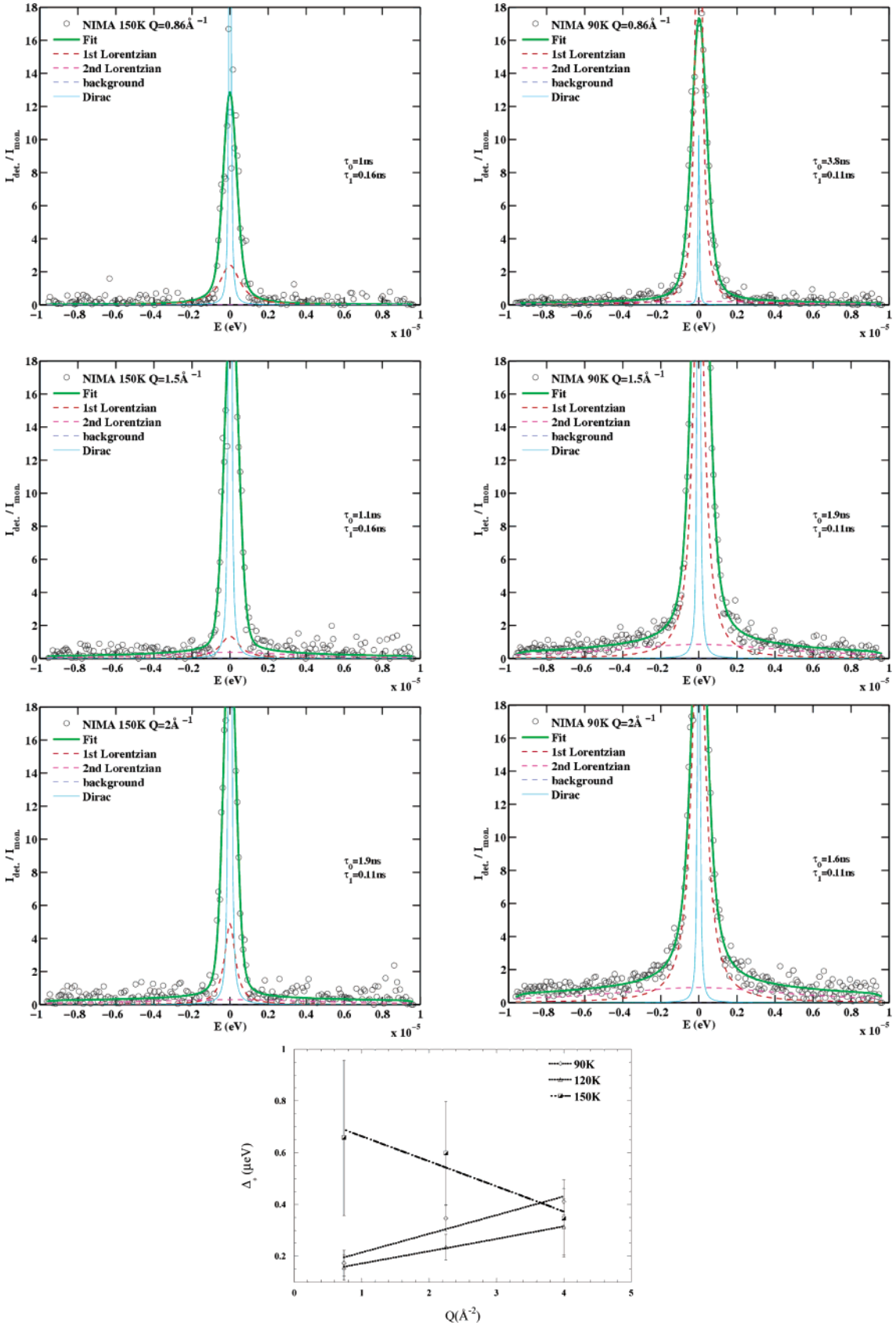

Figure 9. Examples of experimental spectra (○) at selected Q-values for $CH_3CONDCH_3$, $\Delta E = 1$ μeV, together with the best fit (solid line) and the QE components (dotted lines). The background is also shown (short dashed line). The Dirac peak is approximated by a narrow Lorentzian with fixed width. The evolution of the line width (hwhm) of the slower motion as a function of Q^2 of the QE component is shown in the bottom figure. The lines are included as guides for the eye.

component. A better understanding of these new results could be obtained by performing pulsed-field-gradient proton NMR experiments.

However, it has not escaped our attention that at low temperatures it is expected that the motional spectrum of CH_3 groups will be dominated by quantum tunneling, characterized

by a narrow, well-defined inelastic peak with a typical tunneling frequency, τ_t. There is strong evidence for the existence of a universal law for methyl dynamics, suggesting that tunneling frequency depends exponentially on the height of the rotation barrier. Systematic studies of barrier heights and tunneling frequencies of CH_3 groups in the series $CH_3-(CH_3)_n-CO-(CH_2)_m-CH_3$ have shown that methyl groups next to carboxyl groups have low barrier heights.[34] Thus, it may be that in NMA the tunneling lines are as low in energy as those in 2-butadone,[34] methyl acetate,[35] and acetanilide[36] observed up to 0.8 μeV, but unfortunately are resolution-limited in this experiment. As a result, as shown in Figure 7, below 100 K the tunneling motion would dominate but be resolution limited, while above 100 K, once the structure of the tunneling lines has disappeared, the rotational motion of the methyl groups would become more important.

Conclusion

This work aims at a better understanding of the fundamental aspects of peptide and HB, and the methyl groups in NMA. Of the many factors that govern the structure, stability, and functionality of proteins, interactions involving peptide and HB often play a very important role. Peptide bonds hold together the amino acid residues in proteins, covalently linking them together, while HB are present at the substrate binding sites (among others) of enzymes. Simplistically, HB can be explained by the electrostatic attraction between the partial charges on the atoms involved.

The present work indicates that NMA has to be considered as a crystal that presents positional disorder undergoing dynamical transitions. Apart from the evolution of the *a* lattice parameter, which in fact reflects changes of the averaged HB direction, the question of proton transfer between proton donor and acceptor remains unresolved. From our data alone we cannot ascribe in a straightforward way the origin of the coupling behavior of the amide modes to methyl torsions of the NMA. Supposing that some negative charge density is bound to the proton, it is possible to argue that repulsive forces increase as the O···H distance decreases upon cooling and that around 230 K the lattice relaxes without an actual proton transfer. However, the existence of a nonharmonic potential, reflected by the behavior of the generalized density of states and the observation of negative thermal expansion, could be justified by the "vibrational" polaron theory[37,38] in which a dynamic localization of the vibrational energy is created by coupling an internal mode to a lattice phonon.

Using inelastic and quasi-elastic neutron scattering and selectively deuterated samples has made it possible to distinguish contributions arising from different parts of the molecules. Indeed, as discussed in section B under Results and Discussion, activation energy values for the methyl groups show that the dynamical environment of each methyl group is unique. Moreover, combining results from three different spectrometers allowed an extended time and dynamical range to be covered (thus showing that in NMA dynamical disorder persists until around 100 K) and observation of the librational peak as demonstrated in section C of the Results and Discussion section.

Most hydrated proteins undergo a dynamic transition[29,39] in the temperature range of about 200−230 K which is related to an increase in the mean square displacement $\langle u^2 \rangle$, showing a behavior very similar to the one observed in the model NMA system. In the case of proteins, this dynamic transition correlates with the appearance of measurable biochemical activity. Many experimental and computational studies point to solvent dynamics as controlling the dynamic transition in proteins. However, one cannot ignore that a similar transition is also observed in the methyl groups of side chains.[30,40] Doster et al.[21] has suggested that the mechanism underlying such transitions is to some extent an intrinsic property of the constituent elements. Our observation of a very similar dynamical transition in this model system in the absence of any hydration water lends support to this suggestion.

Finally, we note that the ensemble of our results can be taken as an indication that it may be possible using neutron scattering in small-molecule organic crystals, in the absence of solvent molecules, to pursue further studies for understanding the dynamics and kinetics of packing and conformation of systems that form HB patterns, such as amino acids, carboxylic acids, and primary and secondary amides.[41] Such observations are necessary to assess theoretical interaction models used to predict crystal morphology and polymorphism,[42] and are of paramount importance in fields such as pharmacology, solid-state chemistry, and material science.

Acknowledgment. H.N.B. gratefully acknowledges Prof. Elena Boldyreva for her insight on the possibilities of the extension of this work to the study of correlated-structure properties of organic solids that can be used as new materials and devices, including pharmaceutical drugs; and B. Frick for useful discussions. We are grateful to S. Janssen and U. Filges (PSI, Switzerland), Richard M. Ibberson (ISIS, U.K.), and D. Többens (HMI, Berlin) for their assistance during the FOCUS, HRPD, and E9 experiments, respectively. The work performed at the Swiss Spallation Neutron Source SINQ, Paul Scherrer Institut (PSI), Villigen, Switzerland, on FOCUS was partially funded by the BMBF program under Project No. 03-HE4SA2-2 and ff. The experiments performed on E9 benefited from the use of the BENSC at HMI and those on IN10 benefited from the use of the ILL neutron facilities. ISIS is a partner in the EU-supported network of European neutron facilities—the Neutron and Muon Integrated Infrastructure Initiative (NMI3). Work performed at IPNS was funded by the U.S Department of Energy, BES-Materials Science, under Contract No. W-31-109-ENG-38.

References and Notes

(1) Scheiner, S. In *Hydrogen Bonding: A Theoretical Perspective*; Oxford University Press: Oxford, 1997.
(2) Cheatham, T. E., III; Kollman, P. A. *Annu. Rev. Phys. Chem.* **2000**, *51*, 435.
(3) Gumbart, J.; Wang, Y.; Aksimentiev, A.; Tajkhorshid, E.; Schulten, K. *Curr. Opin. Struct. Biol.* **2005**, *15*, 423.
(4) Eckert, J.; Barthès, M.; Klooster, Wim, T.; Albinati, A.; Aznar, R.; Koetzle, T. *J. Phys. Chem. B* **2001**, *105*, 19.
(5) Kearley, G. J.; Johnson, M. R.; Plazanet, M.; Suard, E. *J. Chem. Phys.* **2001**, *115*, 2614.
(6) Mirkin, N. G.; Krimmin, S. J. *J. Mol. Struct.* **1995**, *334*, 3.
(7) Trabelsi, S.; Nasr, S.; Bahri, M.; Bellissent-Funel, M.-C. *J. Phys. Chem. B* **2006**, *110*, 25021.
(8) Katz, J. L.; Post, B. *Acta Crystallogr.* **1960**, *13*, 624.
(9) Hamazaoui, F.; Baert, F. *Acta Crystallogr.* **1994**, *C50*, 757.
(10) Barthès, M.; G. de Nunzio, G.; Ribet, M. *Synth. Met.* **1994**, *76*, 337.
(11) Kearley, J. G.; Johnson, M. R.; Plazanet, M.; Suard, E. *J. Chem. Phys.* **2001**, *115*, 2614.
(12) Dunlop, K. V.; Irvin, R. T.; Hazes, B. *Acta Crystallogr., Sect. D* **2005**, *61*, 80.
(13) Rols, S.; Bordallo, H. N.; Herwig, K. W.; Barthès, M. *Physica B* **2004**, *350*, e-587.
(14) Barthès, M.; Bordallo, H. N.; Eckert, J.; Maurus, O.; de Nunzio, G.; Léon, J. *J. Phys. Chem. B* **1998**, *102*, 6177.
(15) Larson, A. C.; Von Dreele, R. B. In *General Structure Analysis System (GSAS)*; Los Alamos National Laboratory Report LAUR 86-748; 1994.

(16) Janssen, S.; Mesot, J.; Holitzner, L.; Furrer, A.; Hempelmann, R. *Physica B* **1997**, *234*, 1174.
(17) Squires, G. L. In *Introduction to the Theory of Thermal Neutron Scattering*; Dover Publications, Inc.: New York, 1996.
(18) Bradley, K. F.; Chen, S.-H.; Brun, T. O.; Kleb, R.; Loomis, W. A.; Newsam, J. M. *Nucl. Instrum. Methods A* **1988**, *270*, 78.
(19) Bée, M. In *Quasielastic Neutron Scattering: Principles and Applications in Solid State Chemistry, Biology and Materials Science*; Adam Hilger: Bristol, 1988.
(20) Frick, B.; Magerl, A.; Blanc, Y.; Rebesco, R. *Physica B* **1990**, *234*−*236*, 1177.
(21) Doster, W.; Cusak, S.; Petry, W. *Nature* **1989**, *337*, 754.
(22) Evans, J. S. O.; Hu, Z.; Jorgensen, J. D.; Argyriou, D. N.; Short, S.; Sleight, A. W. *Science* **1997**, *61*, 275.
(23) Aasmundtveit, K. E.; Samuelsen, E. J.; Hoffmann, K.; Bakken, E.; Carlsen, P. H. J. *Synth. Met.* **2000**, *113*, 7.
(24) Birkedal, H.; Schwarzenbach, D.; Pattison, P. *Angew. Chem., Int. Ed.* **2002**, *41*, 754.
(25) Barrera, G. D.; Bruno, J. A. O.; Barron, T. H. K.; Allan, N. L. *J. Phys.: Condens. Matter* **2005**, *17*, R217.
(26) Boldyreva, E. V.; Drebushchak, T. N.; Shutova, E. S. *Z. Kristallogr.* **2003**, *218*, 366.
(27) Drebushchak, T. N.; Boldyreva, E. V. *Z. Kristallogr.* **2004**, *219*, 506.
(28) It is always possible to write the dependence of the elastic intensity as a function of the temperature as follows: $I(T) = I(0)\exp(-Q^2[u(T)^2])$, where $u(T)$ is the mean square displacement of the scattering nuclei. Therefore, once the elastic intensity has been experimentally obtained, one can get hold of the variation of $u(T)$.
(29) Daniel, R. M.; Finney, J. L.; Réat, V.; Dunn, R.; Ferrand, M.; Smith, J. C. *Biophys J.* **1999**, *77*, 2184.
(30) Djurado, D.; Combet, J.; Bée, M.; Rannou, P.; Dufour, B.; Pron, A.; Travers, J. P. *Phys. Rev. B* **2002**, *65*, 184202.
(31) Frick, B.; Williams, J.; Trevifio, S.; Erwin, R. *Physica B* **1995**, *213*−*214*, 506.
(32) Chumakov, A. V.; Sergueev, I.; van Bürck, U.; Schirmacher, W.; Asthalterr, T.; Rüffer, R.; Leupold, O.; Petry, W. *Phys. Rev. Lett.* **2001**, *92*, 245508.
(33) Taraskin, S. N.; Loh, Y. L.; Natarajan, G.; Elliott, S. R. *Phys. Rev. Lett.* **2001**, *86*, 1255.
(34) Green, R. M.; Horsewill, A. J. *Mol. Phys.* **1996**, *57*, 887.
(35) Neumann, M. A.; Johnson, M. R.; Aibou, A.; Horsewill, A. J. *Chem. Phys.* **1998**, *229*, 245.
(36) Johnson, M. R.; Prager, M.; Grimm, H.; Neumann, M. A.; Kearley, G. J.; Wilson, C. C. *Chem. Phys.* **1999**, *244*, 49.
(37) Scott, A. C. In *Nonlinear Science*; Oxford University Press: Oxford, 1999.
(38) Scott, A. C.; Bigio, I.; Johnston, C. *Phys. Rev. B* **1989**, *39*, 12883.
(39) Caliskan, G.; Briber, R. M.; Thirumalai, D.; Garcia-Sakai, V.; Woodson, S. A.; Sokolov, A. P. *J. Am. Chem. Soc.* **2006**, *128*, 32.
(40) Frick, B.; Fetters, L. J. *Macromolecules* **1994**, *27*, 974.
(41) Weissbuch, I.; Leiserowitz, J.; Lahav, M. In *Crystallization Technology Handbook*; Mersmann, A., Ed.; Marcel Dekker: New York, 1995. Crystal polymorphism embodies the ability of molecules to form diverse packing arrangements displaying different physical and chemical characteristics.
(42) Bernstein, J. In *Polymorphism in Organic Crystals*; Clarendon: Oxford, 2002.